Multifunctional ternary composites with silver nanowires and titanium dioxide nanoparticles for capacitive sensing and photocatalytic self-cleaning applications

Carmen R. Tubio[a*], Nelson Pereira[b,c], Lia Campos[a], Pedro Manuel Martins[d,e], Jose Luis Vilas-Vilela[a,f], Carlos M. Costa[b,e,g*], Senentxu Lanceros-Mendez[a,h]

[a]*BCMaterials, Basque Center for Materials, Applications and Nanostructures, UPV/EHU Science Park, 48940 Leioa, Spain*

[b]*Physics Centre of Minho and Porto Universities (CF-UM-UP), University of Minho, Campus de Gualtar, 4710-057 Braga, Portugal*

[c]*Centre ALGORITMI, University of Minho, Campus de Azurém, 4800-058 Guimarães, Portugal*

[d]*Centre of Molecular and Environmental Biology, University of Minho, Campus de Gualtar, 4710-057 Braga, Portugal*

[e]*Institute of Science and Innovation for Bio-Sustainability (IB-S), University of Minho, Campus de Gualtar, 4710-057 Braga, Portugal*

[f]*Departamento de Química Física, Facultad de Ciencia y Tecnología, Universidad del País Vasco (UPV/EHU), Apdo. 644, Bilbao, Spain*

[g]*Laboratory of Physics for Materials and Emergent Technologies, LapMET, University of Minho, 4710-053 Braga, Portugal*

[h]*Ikerbasque, Basque Foundation for Science, 48009 Bilbao, Spain*

*carmen.rial@bcmaterials.net

*cmscosta@fisica.uminho.pt

ABSTRACT: Multifunctional polymer composites are of increasing interest as they allow tuning physical-chemical properties for specific applications. A ternary composite material is presented based on the incorporation of titanium dioxide nanoparticles (TiO_2) and conductive silver nanowires (AgNWs) into a poly(vinylidene fluoride) (PVDF) polymer matrix. The films were prepared by solvent casting varying the contents of the filler up to 10 wt.%, showing improved mechanical and dielectric responses and tailorable

optical properties. In contrast, the morphology, polymer phase and thermal stability are nearly independent of the filler type and content within the composite. A dielectric constant up to 14 at 1 kHz was obtained for the 7.5%AgNWs/2.5%TiO_2/PVDF sample. It is demonstrated the (multi)functionality of the developed materials for photocatalytic self-cleaning and capacitive sensing applications, indicating the suitability of the approach for next-generation hybrid multifunctional materials.

KEYWORDS: ***c****apacitive sensing; photocatalysis; PVDF; ternary composites; self-cleaning;*

1. INTRODUCTION

Interest in smart materials-based devices has grown significantly in recent years, playing an increasing role in technological evolution. They are exciting for a wide variety of applications in areas such as biomedicine [1], soft robotics [2], and aerospace [3], among others. The performance of these smart materials directly depends on the operating conditions and integration into the devices, which affects both the selection of materials and the manufacturing process. Therefore, many studies have been focussing on polymer-based composites, as they provide exceptional properties in terms of tailorability of the physical-chemical properties and functional response, together with high design flexibility, among others [4-5].

The proper selection of the polymer matrix and fillers, assuring compatibility, are essential to obtain composites with superior performance. Thermoplastic polymers, based on their processability from the melt and from solution, allow the production of complex 3D structures with high structural performance and improved integration. Among the different thermoplastic polymers, poly(vinylidene fluoride) (PVDF) polymer and co-polymers stand out due to their excellent mechanical, electrical and chemical properties and also for their electroactive properties, including piezo, pyro and ferroelectricity [6-9]. PVDF is a semicrystalline polymer that can crystallise into five crystalline phases (α, β, γ, δ, and ε) depending on the processing conditions [10-12]. For technological applications, the most used phases are α and β. In particular, the β-phase is the one with the largest ferroelectric, piezoelectric, and pyroelectric properties, whereas the α-phase is the most stable one from a thermodynamic point of view when the material is directly obtained from the melt [10-11, 13]. Due to its electroactive properties, PVDF is being used in different

applications, such as sensors and actuators, spin-valve devices, energy harvesting, tissue engineering, and drug delivery carrier systems [6, 8].

As a response to the growing demand for industrial applications, functional fillers are included in specific polymer matrices to improve or induce particular properties. Thus, carbon nanotubes (CNT) [14-15], graphene [15-16] or carbon black [17-18] are used for mechanical reinforcement and for increasing the electrical conductivity; ionic liquids [19-20] to improve ionic conductivity or induce a thermochromic response, for example; magnetic nano- and microparticles [21-22] to induce a magnetic response to the polymer matrix, and metal-organic frameworks (MOFs) [23-24] for tailoring mechanical or dielectric properties and absorption capabilities, among others.

Many advances have been achieved in the enhancement of dielectric response [25], electrochemical properties [26] and electrical conductivity [27] in PVDF-based composites. However, these studies mainly focus on improving or inducing a single functionality in the sample. Therefore, the development of nanocomposites with dual functionality can represent a step forward towards materials applicability, with critical technological benefits in terms of reduced materials use and simplified processing steps by avoiding the use of multiple materials.

Recent examples have shown that the development of PVDF-based composites with dual functionality allows the combination of quite different characteristics. In the area of electronic systems, the combination of fillers with dielectric, magnetic, and electrical conducting properties has been explored, including quantum dots/$CoFe_2O_4$ [28], Fe_3O_4/CNT [29], boron nitride/SiC [23] or CNT/Bi_2O_3 [30]. Among them, PVDF-based composites with dielectric $BaTiO_3$ and magnetic $CoFe_2O_4$ [31] enhance the dielectric response while introducing magnetic responsiveness, suitable for sensing and energy harvesting systems. Despite these promising results, further research is necessary to explore different multi-material combinations, understand structure and properties relationships between fillers, synergetic effects, and control interface between matrix and fillers.

In this work, PVDF-based composites incorporating TiO_2 and Ag nanowires (AgNWs) functional fillers with relative content up to 10 wt.% have been prepared. The selected maximum filler content allows maintaining the samples' structural, mechanical stability and integrity. Mainly, TiO_2 particles are chosen due to their photocatalytic properties [32-33], with well kown potential for environmental remediation [34-35] and energy applications [36-37]. Ag nanowires are selected based on their catalytic, optical, and antimicrobial

properties [38-39]. Combining these fillers with a robust PVDF matrix allows to build up a ternary composite with multifunctional properties.

In particular, the combination of self-cleaning and self-sensing capabilities is relevant in the scope of hygienic surfaces due to the sensing performance for capacitance response in clean environments without dirt and bacteria. Detection and cleaning performance are essential for the next generation smart composites [40]. The developed ternary composites were characterised in terms of microstructure, polymer phase, thermal, optical, mechanical and dielectric properties. Further, the applicability of the multifunctional composite for photocatalytic self-cleaning and capacitive sensing has been demonstrated.

2. EXPERIMENTAL SECTION

2.1 Materials

Poly(vinylidene fluoride), PVDF (Solef 6020, Mw = 700 kg/mol) and the solvent N,N-dimethylformamide (DMF, 99.5%) were purchased from Solvay and Sigma-Aldrich, respectively. Titanium dioxide (TiO_2) nanoparticles were supplied by Evonik Industries AG (Degussa P25) with a surface area ranging from 35 to 65 m^2/g. Silver nanowires (AgNWs) were acquired from ACS Material with a diameter of 90 nm and lengths of 20–30 μm.

2.2 Nanocomposites preparation

PVDF composites with varying contents of AgNWs and TiO_2 were prepared following the general guidelines presented in [9]. First, specific amounts of TiO_2 and AgNWs were uniformly dispersed in 5 mL of N,N-Dimethylformamide (DMF, Anhydrous, 99.8%, Sigma-Aldrich), and the mixture was ultrasonicated for 2 h. Then, 1 g of PVDF was dissolved in the resulting mixture under magnetic stirring for 2 h. Finally, thin films were prepared by doctor-blade and cured in an oven at 210 ºC for 15 min to obtain dense films with a thickness of around 50 μm. For comparison, a pristine PVDF film was prepared according to the above process. The prepared samples with the different filler contents and the corresponding nomenclature, are presented in Table 1.

Table 1. Samples nomenclature and relative percentage of the different fillers in the composite samples.

Samples	Pristine PVDF	10%AgNWs/ PVDF	7.5%AgNWs/ 2.5%TiO_2/PVDF	5%AgNWs/ 5%TiO_2/PVDF	2.5%AgNWs/ 7.5%TiO_2/PVDF	10%TiO_2/ PVDF
PVDF (wt.%)	100	90	90	90	90	90
TiO_2 (wt.%)	0	0	2.5	5	7.5	10
AgNWs (wt.%)	0	10	7.5	5	2.5	0

2.3 Samples characterization

The samples morphology (surface and cross-section) was analysed by Scanning Electron Microscopy (SEM) using Hitachi S-4800. Before analyse, samples were sputtered with 10 nm thin gold layer.

Fourier transform infrared (FTIR) spectra were obtained using an FTIR/ATR spectrometer (Jasco FT/IR-4100). The spectra were recorded in the 4000–600 cm^{-1} wavenumber range for 64 scans with a resolution of 4 cm^{-1}.

Thermogravimetric analysis (TGA) was performed using a TGA/SDTA 851e equipment (Mettler Toledo) between 30 °C and 800 °C at a heating rate of 10 °C/min.

The degree of crystallinity of the composites was examined after Differential Scanning Calorimetry (DSC) measurements in the temperature range of 25 °C to 200 °C at a heating rate of 10 °C/min for cooling and heating (Perkin-Elmer DSC 8000 instrument).

UV-visible transmittance spectra were obtained in the wavelength region from 200 to 800 nm using a spectrophotometer (Cary 60 UV-vis Agilent Technologies).

Mechanical properties of the composites were carried out in stand-alone films with an AGS-X Universal Testing Machine from Shimadzu in tensile testing at 1 mm/min. Samples dimensions for mechanical tests are 15 mm long, 6-8 mm width and 50 μm thick. Young's modulus (E), strain (ε_b) and stress (σ_b) at break were determined. At least 4 speciments of each sample were evaluated to obtain the mean value and standard deviation of the mechanical parameters.

The dielectric response of the samples was obtained under the same experimental conditions by measuring the capacity (C) and tan δ using a Quadtech 1929 Precision LCR meter at room temperature in the frequency range from 200 Hz to 1 MHz at an applied voltage of 0.5 V. Before the measurements, gold circular electrodes of 5 mm diameter were deposited onto both sides by magnetron

sputtering SC502 sputter coater of each composite to form a parallel plate capacitor. The real part of the dielectric constant (ε') and the AC conductivity (σ') was calculated by [41]:

$$\varepsilon' = \frac{C \cdot d}{A \cdot \varepsilon_0} \quad (1)$$

$$\sigma' = \varepsilon_0 \omega \varepsilon'' \quad (2)$$

Where C is the capacitance (F), ε_0 ($8.85 \cdot 10^{-12}$ F/m) is the permittivity of free space, $\varepsilon'' = \tan\delta \cdot \varepsilon'$ is the imaginary part of the dielectric constant, d is thickness, A is area of the electrodes and $\omega = 2\pi\nu$ is the angular frequency.

2.4. Functional photocatalytic self-cleaning and capacitive sensing performance

The photocatalytic activity of the sample was evaluated using a methylene blue (MB - 1×10^{-5} M) solution at pH 6.8 in contact with the nanocomposite under UV light irradiance of 0.33 mW/cm^2- eight lamps (Philips 8W) maximum irradiation peak at 365 nm [32]. The MB absorbance solution was monitored in the range 450−750 nm at different times using a Shimadzu UV-2501PC UV/Vis spectrophotometer. The MB photodegradation rate was monitored through the absorption peak at 663 nm.

Concerning the capacitive sensing evaluation, the ternary composite film was sandwiched between two ITO conductive-coated PET electrode films with an active area of 30 mm x 7 mm and connected to the application circuit via alligator clips, as shown in Figure 1.

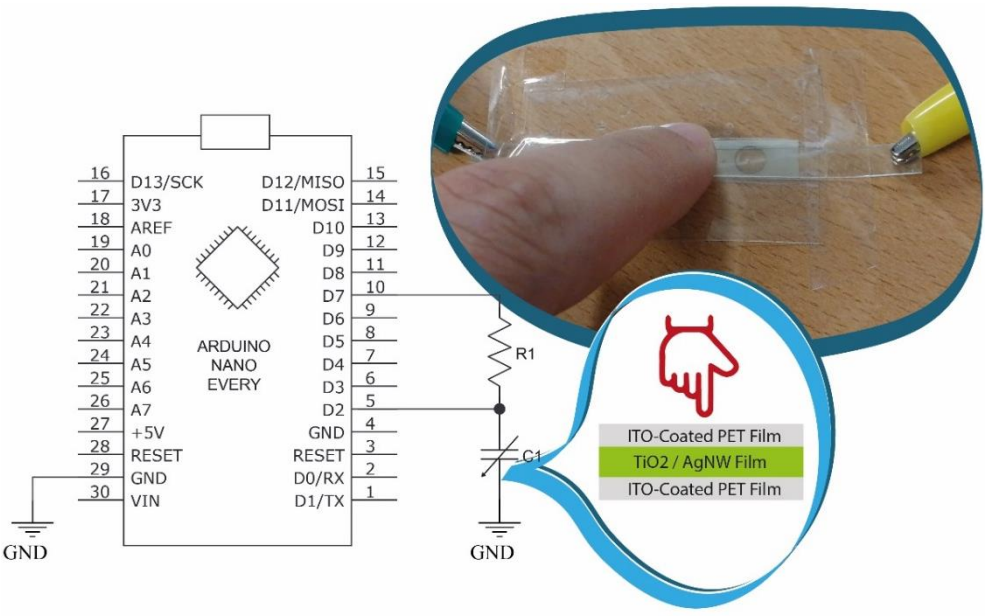

Figure 1. Schematic representation of the sample and electronic circuit for capacitive sensing evaluation.

The application is composed of an Arduino nano every board with an ATMEGA4809 microcontroller running at 20 MHz. The microcontroller connects to a PC with a baud rate of 9600 bps, and the data are plotted in a QT 5 application.

The microcontroller measures the time the capacitive sample takes to charge. First, the microcontroller connects the D2 pin to the ground discharging the sensor, and then the D2 pin waits for the logic level to be high, as Pin D7 is set to VCC [42]. When D2 detects the high logic level, the microcontroller measures the time since the beginning of the charging of the capacitive sample.

3. RESULTS AND DISCUSSION

3.1 Morphology, optical properties, polymer phase, thermal, and mechanical characteristics

The microstructure of the ternary composite samples was investigated using SEM, and representative images are shown in Figure 2. The cross-sectional SEM images of pristine PVDF and PVDF composites with different AgNW and TiO_2 filler contents (Figure 2a-f) show a compact morphology without filler aggregation that demonstrates excellent compatibility and distribution of the different fillers within the polymer matrix. This fact is corroborated by the corresponding surface images in the insets where the spherulite structure the PVDF is observed. Also, the surface show that the filler type and content affects the spherulitic structure, influencing threfore the polymer crystallization process [43]. In particular, Figure 2a and 2b show homogeneous and dense morphology without pores for pristine PVDF and 10%AgNWs/PVDF samples, respectively. Regarding the microstructure of the ternary composite samples with TiO_2 filler, a rougher surface was observed with TiO_2 particles randomly dispersed in the polymer matrix without agglomeration. Regardless of the filler type and content, the polymer matrix mantains the typicall microstructure.

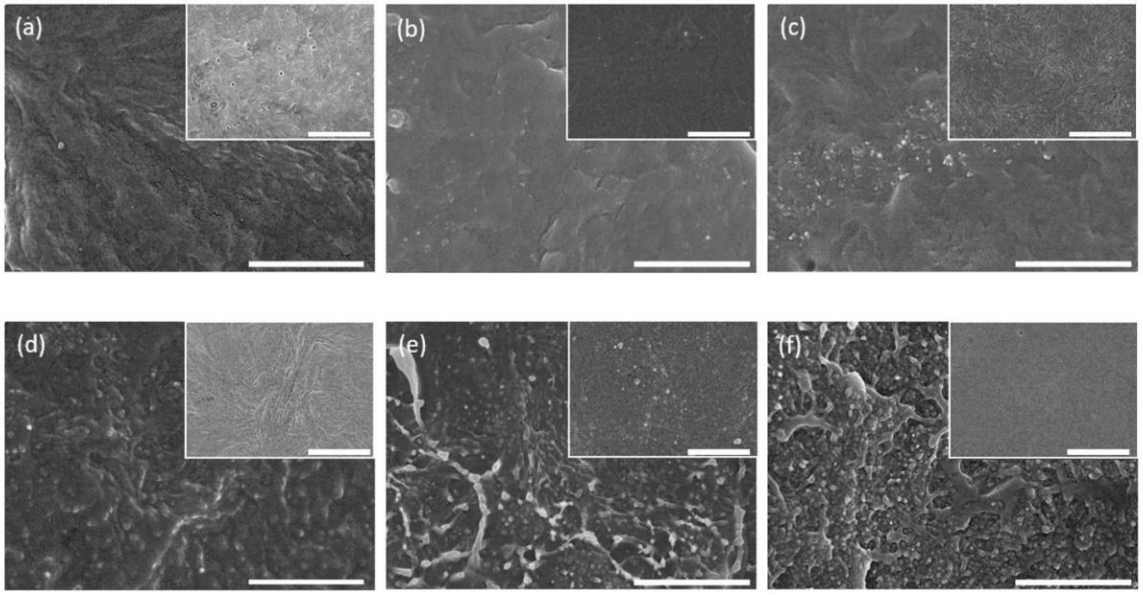

Figure 2. Cross-sectional and surface (inset) SEM images of PVDF composites with different filler contents. (a) pristine PVDF (b) 10%AgNWs, (c) 7.5%AgNWs/2.5%TiO_2, (d) 5%AgNWs/5%TiO_2, (e) 2.5%AgNWs/7.5%TiO_2, (f) 10%TiO_2. Scale bars represent 2 μm.

The UV-vis transmittance spectra of the different samples were recorded to quantify the optical transparency of the samples and UV absorption, as shown in Figure 3.

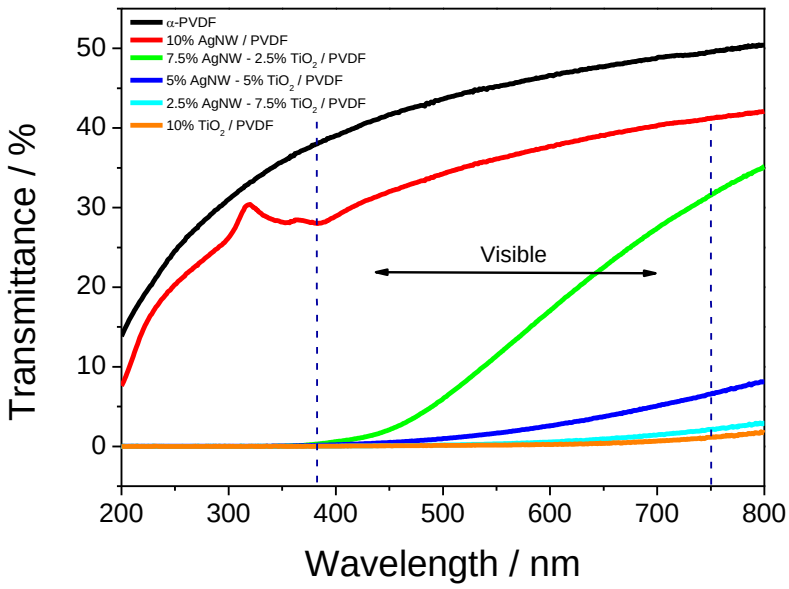

Figure 3. UV-vis spectra of the PVDF composites with different fillers.

Pristine PVDF shows higher transmittance than the rest of the samples in the ultraviolet-visible (UV-vis) (Figure 3), with a optical trasmittance of ~ 45% in the λ = 540−560 nm region. The addition of any filler causes a reduction in the transparency of the composite, being more striking with a higher TiO_2 content in than for the AgNW filler. For 10%AgNWs/PVDF sample, a peak at ~340 nm is observed, related to the plasmon peak [44]. It is to notice that this peak is not detected for the other composite samples due to the overall reduction of the optical transmittance. Composite films with TiO_2 show a yellow/brown tinge, which increases with filler content reducing the transmittance in the visible region and improving the absorbance in the UV region. This behaviour is essential for the photocatalytic activity of the composite under UV irradiation.

Fourier transform infrared (FTIR) spectroscopy was performed to analyse the presence of α and β phases in the composites, as shown in Figure 4a. Vibration bands at 766 and 973 cm^{-1} are ascribed to the α-phase, whereas the peaks at 840 and 1270 cm^{-1} correspond to the β-phase [45]. Furthermore, it is evidenced that the intensity of the peak at 840 cm^{-1} for the sample with the highest TiO_2 content is sharper than the corresponding peak in the pristine PVDF spectra. The electroactive β-phase content of PVDF was quantified taking into consideration the characteristic absorption bands of α (766 cm^{-1}) and β (840 cm^{-1}) PVDF by applying equation 3 [45]:

$$F(\beta)=\frac{A_\beta}{\left(\frac{K_\beta}{K_\alpha}\right)A_\alpha+A_\beta} \quad (3)$$

where A_α and A_β are the absorbances at 766 and 840 cm^{-1} respectively, and K_α ($6.1\cdot10^4$ cm^2/mol) and K_β ($7.7\cdot10^4$ cm^2/mol) are the corresponding absorption coefficients [45]. Table 2 shows the β-phase content for pristine PVDF and PVDF composites with different AgNWs and TiO_2 contents, the maximum electroactive phase content being 14%.

Table 2. β-phase content and degree of crystallinity obtained from FTIR spectra and DSC themograms.

Samples	β phase ± 2 (%)	Xc ± 2 (%)
Pristine PVDF	4	43
10%AgNWs/PVDF	3	46
7.5%AgNWs/2.5%TiO_2/PVDF	10	46
5%AgNWs/5%TiO_2/PVDF	5	43
2.5%AgNWs/7.5%TiO_2/PVDF	3	39
10%TiO_2/PVDF	14	39

It has been reported that the addition of TiO_2 leads to an increase in the β-phase content of PVDF [46], whereas the addition of AgNWs beyond 2.5 % prevents the formation of β-phase [47]. Table 2 shows that one filler compensates the effect of the other, leading to low electroactive phase contents for the ternary composites, except for the case of the 7.5%AgNWs/2.5%TiO_2/PVDF sample, which shows a higher β-phase value. This fact can be ascribed to improved dispersion of the low TiO_2 content as shown in the SEM images and, therefore, to an increased contact area with the polymer matrix, which leads to increased β-phase content.

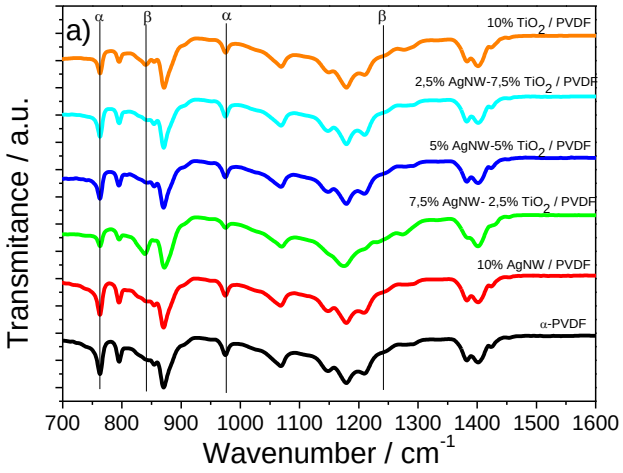

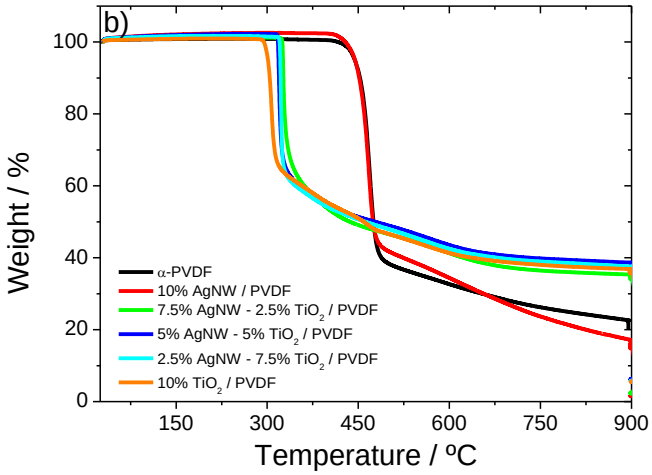

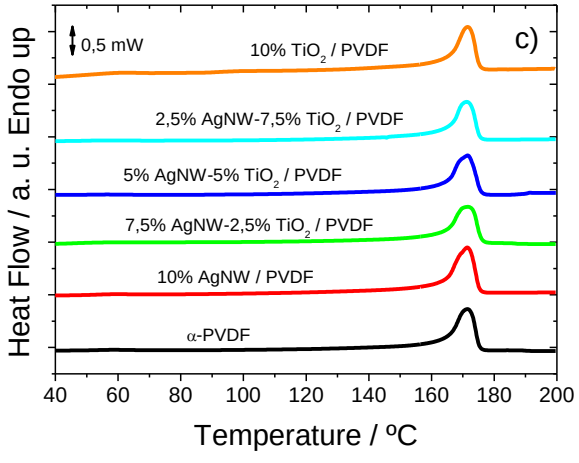

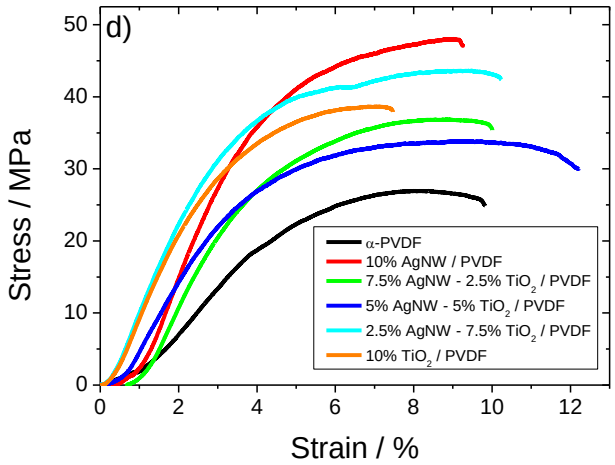

Figure 4. (a) FTIR spectra, (b) TGA curves, (c) heating DSC curves, and (d) Stress-strain curves for pristine PVDF and PVDF composites with different AgNWs and TiO_2 contents.

TGA tests were carried out to analyse the thermal decomposition of the different samples and to evaluate the effect of the fillers on the thermal stability of the composites. TGA thermograms for the different samples are shown in Figure 4b. All samples show a similar thermal degradation profile: a multi stage-process weight loss, except for pristine PVDF, which only displays a single degradation corresponding to the depolymerisation of the –CH_2-CF_2- chains [48]. The presence of TiO_2 within the polymer matrix leads to a substantial reduction in the polymer degradation temperature. In particular, onset temperature degradation, defined as the slope changes as the composite begins to decompose, values of composites with TiO_2 decrease from around 450 ºC for the pristine PVDF and 10% AgNWs/PVDF samples down to 350 ºC. This fact is possibly due to an oxidative decomposition of the material caused by the catalytic effect of the metal oxide [49]. Consequently, the presence of TiO_2 triggers lower thermal stability. Furthermore, the total weight loss of the composite with TiO_2 is lower than the composites without it. The former ones have a weight loss of 60%, which increase to 75% for the pristine PVDF sample, and then further increase to 80% with the addition of 10% AgNWs content. This increase in the residual mass can be ascribed to products resulting from the chelating ligands of titanium ion and fluoride produced by the backbone homolysis in the PVDF decomposition [50]. A slight reduction of the residual mass is observed for the AgNW containing composite, which indicates possible secondary reactions of the PVDF degradation products with the AgNW filler.

Differential scanning calorimetry (DSC) has been used to evaluate the thermal properties of the samples (Figure 4c). It is observed that the addition of fillers does not lead to any relevant variation of the melting temperature of the crystalline phase of PVDF. Thus, all samples are characterized by just one melting peak around 170 ºC, corresponding to a predominance of α phase, confirming the FTIR results (Figure 4c). In addition, the degree of crystallinity (Table 2) was evaluated after equation 4:

$$X_c = \frac{\Delta H}{\Delta H_\alpha \cdot x + \Delta H_\beta \cdot y} \quad (4)$$

where ΔH is the melting enthalpy of the sample, ΔH_α (93.07 J/g) and ΔH_β (103.4 J/g) are the melting enthalpies of the α and β phases, and x and y correspond to the amount of the α and β phases present in the sample and calculated after the FTIR results, respectively [45]. The degree of crystallinity of the samples depends on the filler type and content. On the one hand, increasing the amount of TiO_2 hinders PVDF crystals growth [51]. On the other hand, it has been reported that AgNWs has no influence on the crystallisation of the composite [52], but it seems that increasing the content of this filler has a beneficial effect on the degree of crystallinity of samples. Therefore, the lower the content of TiO_2, and the higher the amount of AgNWs, the larger the degree of crystallinity of the samples.

The mechanical behavior was evaluated after stress-strain tests in the tensile mode, as presented in Figure 4d, and Table 3 summarises the mechanical parameters obtained from the measured curves. Regardless of the filler type and its content, composites present the typical mechanical behaviour of thermoplastic polymers, composed by the elastic and the plastic region, divided by the yielding point [53]. Furthermore, it is observed that the composite samples show an increase in mechanical behaviour compared to pristine PVDF, in which the fillers act as a mechanical reinforcement. From Table 3, it can be seen that the Young's modulus, determined by the tangent method in the elastic region at 3% of the maximum elongation [54], increases with the addition of the TiO_2 filler, where TiO_2 enhances the mechanical behaviour due to the strong interfacial interaction between TiO_2 nanoparticles and polymer matrix resulting in better dispersion and also a greater surface area of interaction of TiO_2 filler in the matrix. Furthermore, for ternary composite with high AgNWs content (7.5 and 10 wt.%), the Young´s modulus decreases compared to pristine PVDF due to the poor interfacial adhesion and dispersion between this filler and polymer matrix as verified through the SEM images (Figure 2) [55-56].

Table 3. Mechanical parameters of pristine PVDF and PVDF composites with different AgNWs and TiO_2 contents.

Samples	E (MPa)	ε_b (%)	σ_b (MPa)
Pristine PVDF	618 ± 103	10 ± 3	27 ± 6
10%AgNWs/PVDF	393 ± 49	10 ± 1	47 ± 3
7.5%AgNWs/2.5%TiO_2/PVDF	576 ± 124	9 ± 1	37 ± 13
5%AgNWs/5%TiO_2/PVDF	672 ± 115	10 ± 1	34 ± 4
2.5%AgNWs/7.5%TiO_2/PVDF	690 ± 36	10 ± 1	43 ± 1
10%TiO_2/PVDF	750 ± 14	7 ± 1	37 ± 1

This fact is also demonstrated by the stress at break (σ_b) values, as shown in Table 3. The strain at break (ε_b) values are the same for all composites, independently of filler type and content, being also similar to the one observed for pristine PVDF.

3.2 Electrical properties

For capacitive sensing applications, the evaluation of the dielectric properties is essential, and Figure 5 shows the dielectric constant, tan δ and AC conductivity as a function of frequency from 200 Hz to 1 MHz for pristine PVDF and PVDF composites with different AgNWs and TiO_2 contents.

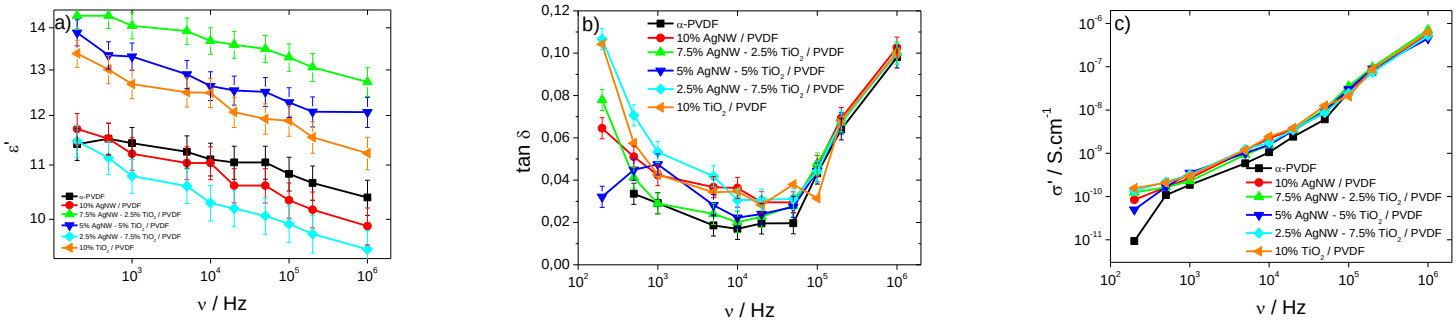

Figure 5. (a) ε', (b) tan δ, and (c) σ' for pristine PVDF and PVDF composites with different AgNWs and TiO_2 contents.

Regardless of the composite type, Figure 5a shows that the dielectric constant (ε') decreases with increasing frequency. This is due to the limited dipolar mobility and the Maxwell-Wagner-Sillars effect. On the other hand, it is observed that the type of filler and its content affects the dielectric behaviour and that the filler that contributes at most in improving the dielectric constant is TiO_2. For ternary composites with low TiO_2 content (2.5 and 5 wt.%), it is observed higher dielectric constants, 14 and 13.3, when compared to pristine PVDF, 11 at 1 kHz. The main reason for this behaviour is due to the interfacial polarisation or Maxwell-Wagner-Sillars (MWS) effect [57-58]. Furthermore, for these samples, it is observed that the filler-filler interaction is predominant when compared to just a filler, leading to improved molecular mobility by interfacial polarisation and consequently the dielectric constant [59]. Furthermore, for the samples with 10% AgNW/PVDF and 2.5% AgNW-7.5%TiO_2/PVDF, it is observed that the dielectric constant decreases when compared to pristine PVDF due to the electric conduction properties of the AgNW filler.

Figure 5b shows that the tan δ as a function of frequency is similar for all samples, regardless of filler type and content. Also, it is detected two different behavior as a function of frequency in which the tan δ decreases with increasing the frequency up to 10^4 Hz. From Figure 5b, it is observed that tan δ increases with frequency for high-frequency regions (above 10^4 Hz) ,which can be attributed to the molecular motion of crystalline-amorphous interfaces chain segments [60].

Figure 5c shows the AC conductivity values for all composites as a function of frequency, and we can see that conductivity increasing with increasing frequency. Furthermore, it is detected that filler addition improves the AC conductivity at low frequencies compared to pristine PVDF, which can be explained by the space charge polarization that occurs on the nanocomposite samples.

Figure 5c shows a single regime in the conductivity behaviour regardless of the frequency range, assigned to ac conductivity [61]. Considering that the AC conductivity behaviour is frequency dependent, it can be described by Jonscher's universal law [62]:

$$\sigma'(\omega) \propto \omega^n \quad (5)$$

where ω is the angular frequency and the n parameter characterises a thermally activated hopping across an energy barrier ($0 < n < 1$). The frequency exponent n is obtained by fitting the experimental data and its value ranges between 0.85 and 1 for all samples, independently of filler type and content, which confirms that the conduction mechanism in the samples is dominated mainly by hopping [59].

3.3 Photocatalytic self-cleaning and capacitive sensing functional response

The sample 5%AgNWs/5%TiO_2/PVDF was placed in contact with an MB solution under UVA irradiation to confirm whether the produced samples exhibit photocatalytic activity. The obtained results and pictures of the samples during the assay are presented in Figure 6.

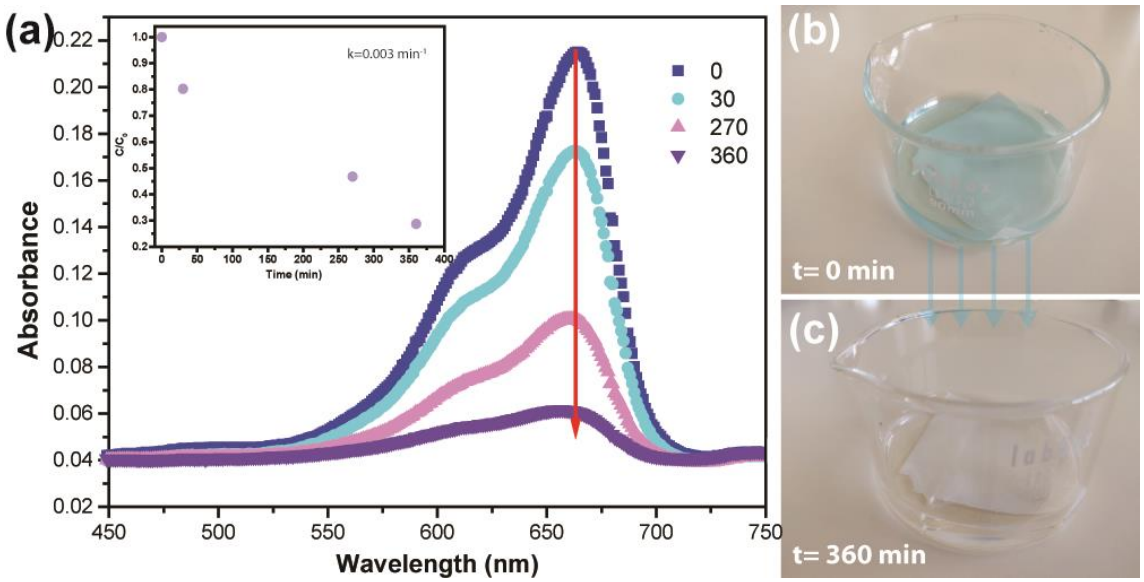

Figure 6. Photocatalytic degradation of MB in solution (1×10^{-5} M and pH=6.5) using the 5%AgNWs/5%TiO_2/PVDF sample, under 360 min of UVA radiation – inset presents the photocatalytic degradation kinetic and the apparent reaction rate (*k*). (a). Pictures of the 5%AgNWs/5%TiO_2/PVDF sample in contact with the MB aqueous solution before (b) and after (c) 360 min of UVA irradiation.

Figure 6a shows the absorbance spectra of MB at different times of contact with the 5%AgNWs/5%TiO_2/PVDF sample, and it is possible to observe a decrease of the maximum absorbance peak of MB (663 nm) over time. Thus, approximately 72% of the MB molecules in solution were removed during 360 min at an apparent reaction rate (*k*) of 0.003 1/min. The MB solution visual inspection after UVA irradiation (Figure 6b and c) confirms that photocatalytic activity occurred as the solution becames colourless. The remarkable ability of sample 5%AgNWs/5%TiO_2/PVDF to absorb UV radiation, indicated in Figure 3, is mainly associated with TiO_2 nanoparticles in the PVDF matrix. The absorption of UVA radiation by the TiO_2 nanoparticles initiates the formation of electron-hole pairs that will react with OH^-, O_2 and H_2O to produce reactive oxygen species (ROS) such as hydroxyl radical (OH•), superoxide radical anions (O_2•−), and hydrogen peroxide (H_2O_2) that attack the MB molecules adsorbed into TiO_2 nanoparticles surface [33, 63]. These same chemical species are also responsible for the self-cleaning effect of TiO_2 nanoparticles. In this way, by degrading organic contaminants, the surface of the 5%AgNWs/5%TiO_2/PVDF sample can clean itself under UV irradiation, avoiding expensive maintenance and extended durability of materials [63-64]. This feature is exciting, considering that the capacitive functionality of this material requires a fingers touch that

promotes surface contamination that can accelerate the material deterioration and electric response.

Considering the high dielectric constant of the 5%AgNWs/5%TiO_2/PVDF sample, Figure 7 shows the sensor response upon repeated applied pressure by finger touch, as shown in Figure 1 (see supplementary information Video SV1). The working mechanism of this sensor is due to the finger approaching the dielectric material, leading to an increase of capacity. When a finger gets close to the nanocomposite, the capacity increases from 81.7 pF to approximately 200 pF, which is enough to detect a touch event. In Figure 7, different regions are defined: 1) no-touch, 2) touch, and 3) increased touch pressure and, consequently, enlarged touch area. The response of this capacitive sensor does not show clamping effects, hysteresis, or degradation over time, demonstrating adequate mechanical stability (Figure 7).

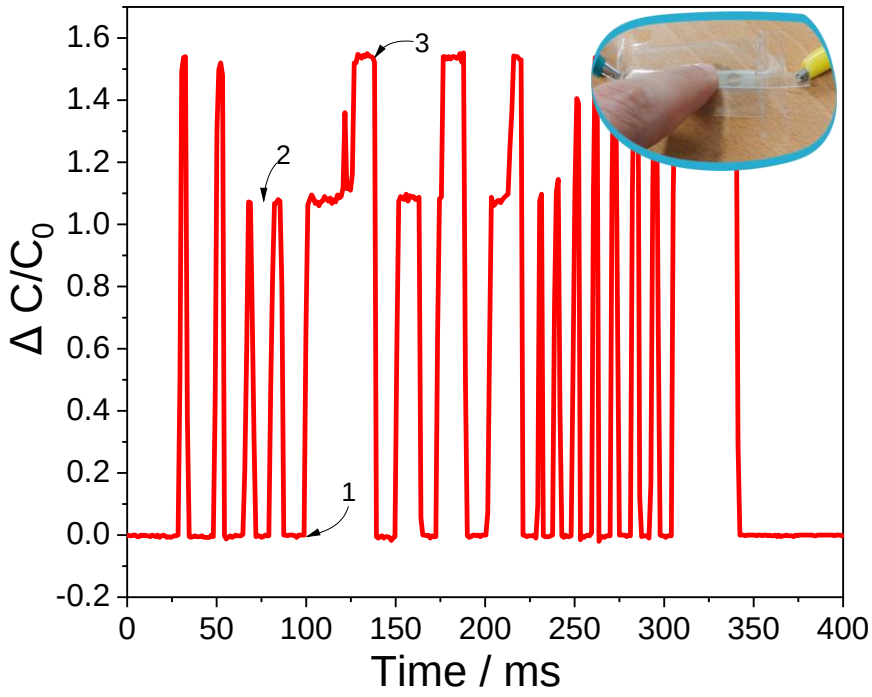

Figure 7. Demonstration of the capacitive sensor response upon repeating finger touch.

Considering the photocatalytic self-cleaning behaviour and the excellent capacitive response of this composite material for environmental cleaning and sense, it is demonstrated that it is possible to obtain a multifunctional PVDF-based material with multifunctional capabilities based on the inclusion of two complementary fillers at low filler content.

4. CONCLUSIONS

Hybrid materials with both self-cleaning and capacitive sensing capabilities have been developed. The ternary composites were produced by solvent casting technique based on titanium dioxide nanoparticles (TiO_2) and silver nanowires (AgNWs) in a poly(vinylidene fluoride) (PVDF) matrix with different contents of both fillers. The morphology of these composites is compact, and the fillers are well dispersed. The filler type and its content does not affect the polymer phase and the thermal properties. The optical properties are determined by TiO_2 filler versus AgNW filler with higher absorbance. Furthermore, the Young's Modulus of the composites increases with increasing TiO_2 content and decreases with the inclusion of AgNW content (7.5 and 10 wt.%).

Dielectric constants up to 14 at 1 kHz have been obtained for the 7.5%AgNWs/2.5%TiO_2/PVDF sample.

The photocatalytic activity was proved for sample 5%AgNWs/5%TiO_2/PVDF by removing ≈ 70% of MB in solution under 360 min of UVA irradiation; additionally, the ROS generation necessary for the photocatalytic process allows to foresee a self-cleaning ability. The capacitive sensing capability has been demonstrated with excellent functional response for the same sample.

This work demonstrates that it is possible to develop multifunctional materials based on two different fillers with tailored functional responses (photocatalytic self-cleaning and capacitive behaviour) for the next generation smart materials.

ASSOCIATED CONTENT

Supporting Information

Video SV1: Video for sensor response upon repeated finger touch.

AUTHOR INFORMATION

Corresponding authors

Carmen R. Tubio - *BCMaterials, Basque Center for Materials, Applications and Nanostructures, UPV/EHU Science Park, 48940 Leioa, Spain;* https://orcid.org/0000-0002-6988-8242; Email: carmen.rial@bcmaterials.net

Carlos M. Costa - *Physics Centre of Minho and Porto Universities (CF-UM-UP), University of Minho, Campus de Gualtar, 4710-057 Braga, Portugal; Institute of Science and Innovation for Bio-Sustainability (IB-S), University of Minho, Campus de Gualtar,*

4710-057 Braga, Portugal; Laboratory of Physics for Materials and Emergent Technologies, LapMET, University of Minho, 4710-053 Braga, Portugal; https://orcid.org/0000-0001-9266-3669; Email: cmscosta@fisica.uminho.pt

Authors

Nelson Pereira - *Physics Centre of Minho and Porto Universities (CF-UM-UP), University of Minho, Campus de Gualtar, 4710-057 Braga, Portugal; Centre ALGORITMI, University of Minho, Campus de Azurém, 4800-058 Guimarães, Portugal;* ; https://orcid.org/0000-0003-1293-0865

Lia Campos - *BCMaterials, Basque Center for Materials, Applications and Nanostructures, UPV/EHU Science Park, 48940 Leioa, Spain;* https://orcid.org/0000-0001-6393-4423

Pedro Manuel Martins - *Centre of Molecular and Environmental Biology, University of Minho, Campus de Gualtar, 4710-057 Braga, Portugal; Institute of Science and Innovation for Bio-Sustainability (IB-S), University of Minho, Campus de Gualtar, 4710-057 Braga, Portugal;* https://orcid.org/0000-0001-8179-8242

José Luis Vilas-Vilela - *BCMaterials, Basque Center for Materials, Applications and Nanostructures, UPV/EHU Science Park, 48940 Leioa, Spain; Departamento de Química Física, Facultad de Ciencia y Tecnología, Universidad del País Vasco (UPV/EHU), Apdo. 644, Bilbao, Spain;* https://orcid.org/0000-0002-0188-4579

Senentxu Lanceros-Mendez - *BCMaterials, Basque Center for Materials, Applications and Nanostructures, UPV/EHU Science Park, 48940 Leioa, Spain; Ikerbasque, Basque Foundation for Science, 48009 Bilbao, Spain;* https://orcid.org/0000-0001-6791-7620

Author Contributions

The manuscript was written through contributions of all authors. All authors have given approval to the final version of the manuscript

Notes

The authors declare no competing financial interest.

ACKNOWLEDGMENTS

The authors thank the Fundação para a Ciência e Tecnologia (FCT) and COMPETE 2020 for financial support under the framework of Strategic Funding grants UID/FIS/04650/2021, UID/EEA/04436/2021 and UIDB/04650/2020 and under projects POCI-01-0145-FEDER-028157 and PTDC/FIS-MAC/28157/2017. The authors also thank the FCT for financial support under grant SFRH/BD/131729/2017 (NP) and the investigator contracts 2020.02802.CEECIND (PMM) and 2020.04028.CEECIND (CMC). Financial support from the Basque Government Industry Department under the ELKARTEK program is acknowledged. L. Campos thanks the University of Basque Country (UPV/EHU) for doctoral grant PIFI20/04. Technical and human support provided by SGIker (UPV/EHU, MICINN, GV/EJ, EGEF and ESF) is gratefully acknowledged. The authors would like to thank Asma Mooti for technical assistance.

REFERENCES

1. Genchi, G. G.; Marino, A.; Tapeinos, C.; Ciofani, G. Smart Materials Meet Multifunctional Biomedical Devices: Current and Prospective Implications for Nanomedicine. *Frontiers in bioengineering and biotechnology* **2017,** *5*, 80.

2. El-Atab, N.; Mishra, R. B.; Al-Modaf, F.; Joharji, L.; Alsharif, A. A.; Alamoudi, H.; Diaz, M.; Qaiser, N.; Hussain, M. M. Soft Actuators for Soft Robotic Applications: A Review. *Advanced Intelligent Systems* **2020,** *2*, 2000128.

3. Basheer, A. A. Advances in the Smart Materials Applications in the Aerospace Industries. *Aircraft Engineering and Aerospace Technology* **2020,** *92*, 1027-1035.

4. Oladele, I. O.; Omotosho, T. F.; Adediran, A. A. Polymer-Based Composites: An Indispensable Material for Present and Future Applications. *International Journal of Polymer Science* **2020,** *2020*, 8834518.

5. Cherusseri, J.; Pramanik, S.; Sowntharya, L.; Pandey, D.; Kar, K. K.; Sharma, S. D. Polymer-Based Composite Materials: Characterizations. *Composite Materials: Processing, Applications, Characterizations* **2017,** 37-77.

6. Saxena, P.; Shukla, P. A Comprehensive Review on Fundamental Properties and Applications of Poly(Vinylidene Fluoride) (Pvdf). *Advanced Composites and Hybrid Materials 2021 4:1* **2021,** *4*, 8-26.

7. Ebnesajjad, S. Introduction to Fluoropolymers: Materials, Technology, and Applications. *Introduction to Fluoropolymers: Materials, Technology, and Applications* **2013,** 1-325.

8. Chapter 1 - Electroactive Poly(Vinylidene Fluoride)-Based Materials: Recent Progress, Challenges, and Opportunities | Elsevier Enhanced Reader.

9. Ribeiro, C.; Costa, C. M.; Correia, D. M.; Nunes-Pereira, J.; Oliveira, J.; Martins, P.; Gonçalves, R.; Cardoso, V. F.; Lanceros-Méndez, S. Electroactive Poly(Vinylidene Fluoride)-Based Structures for Advanced Applications. *Nature Protocols* **2018,** *13*, 681-704.

10. Nalwa, H. S. *Ferroelectric Polymers: Chemistry, Physics, and Applications*. M. Dekker, Incorporated: **1995**.

11. Lovinger, A. J. Developments in Crystalline Polymers. Basset, D. C., Ed. Elsevier: London, **1982**.

12. Gregorio, J. R.; Cestari, M. Effect of Crystallization Temperature on the Crystalline Phase Content and Morphology of Poly(Vinylidene Fluoride). *Journal of Polymer Science Part B: Polymer Physics* **1994,** *32*, 859-870.

13. Rasmussen, L. *Electroactivity in Polymeric Materials*. Springer: **2012**.

14. Twinkle; Kaur, M.; Gowsamy, J. K.; Kumar, P.; Kumar, S. Synthesis and Characterization of Cnt/Pvdf Paper for Electronic and Energy Storage Applications. *Emergent Materials* **2020,** *3*, 181-185.

15. Vicente, J.; Costa, P.; Lanceros-Mendez, S.; Abete, J. M.; Iturrospe, A. Electromechanical Properties of Pvdf-Based Polymers Reinforced with Nanocarbonaceous Fillers for Pressure Sensing Applications. *Materials* **2019,** *12*, 3545.

16. Zhang, H.; Zhu, Y.; Li, L. Fabrication of Pvdf/Graphene Composites with Enhanced Beta Phase Via Conventional Melt Processing Assisted by Solid State Shear Milling Technology. *RSC advances* **2020,** *10*, 3391-3401.

17. Ram, R.; Soni, V.; Khastgir, D. Electrical and Thermal Conductivity of Polyvinylidene Fluoride (Pvdf) – Conducting Carbon Black (Ccb) Composites: Validation of Various Theoretical Models. *Composites Part B: Engineering* **2020,** *185*, 107748.

18. Wang, Y.; Xie, J.; Wang, X. The Ultra-Flexible Films of Super Conductive Carbon Black/Poly(Vinylidene Fluoride) as Electrothermal Materials. *Materials Research Express* **2019,** *6*, 116402.

19. Correia, D. M.; Sabater i Serra, R.; Gómez Tejedor, J. A.; de Zea Bermudez, V.; Andrio Balado, A.; Meseguer-Dueñas, J. M.; Gomez Ribelles, J. L.; Lanceros-Méndez, S.; Costa, C. M. Ionic and Conformational Mobility in Poly(Vinylidene Fluoride)/Ionic Liquid Blends: Dielectric and Electrical Conductivity Behavior. *Polymer* **2018,** *143*, 164-172.

20. Sarkar, R.; Kundu, T. K. Density Functional Theory Studies on Pvdf/Ionic Liquid Composite Systems. *Journal of Chemical Sciences 2018 130:8* **2018,** *130*, 1-18.

21. Sanida, A.; Velmachos, T. G.; Stavropoulos, S. G.; Psarras, G. C.; Tsonos, C.; Kanapitsas, A.; Soin, N.; Siores, E. Thermomechanical Response of Fe3o4/Pvdf Nanocomposites. *Procedia Structural Integrity* **2018,** *10*, 91-96.

22. Supriya, S.; Kumar, L.; Kar, M. Optimization of Dielectric Properties of Pvdf–Cfo Nanocomposites. *Polymer Composites* **2019,** *40*, 1239-1250.

23. Wang, B.; Yin, X.; Peng, D.; Zhang, Y.; Wu, W.; Gu, X.; Na, B.; Lv, R.; Liu, H. Highly Thermally Conductive Pvdf-Based Ternary Dielectric Composites Via Engineering Hybrid Filler Networks. *Composites Part B: Engineering* **2020,** *191*, 107978.

24. Valverde, A.; Gonçalves, R.; Silva, M. M.; Wuttke, S.; Fidalgo-Marijuan, A.; Costa, C. M.; Vilas-Vilela, J. L.; Laza, J. M.; Arriortua, M. I.; Lanceros-Méndez, S.; Fernández De Luis, R. Metal−Organic Framework Based Pvdf Separators for High Rate Cycling Lithium-Ion Batteries. *ACS Appl. Energy Mater* **2020,** *2020*, 11907-11919.

25. Feng, Y.; Zhou, F.; Bo, M.; Huang, Y.; Deng, Q.; Peng, C. Enabling High Dielectric Response in Pvdf/V2c Mxene–Tio2 Composites Based on Nontypical V–F–Ti Bonding and Fermi-Level Overlapping Mechanisms. *The Journal of Physical Chemistry C* **2020,** *124*, 27780-27789.

26. Mejri, R.; Dias, J. C.; Hentati, S. B.; Martins, M. S.; Costa, C. M.; Lanceros-Mendez, S. Effect of Anion Type in the Performance of Ionic Liquid/Poly(Vinylidene Fluoride) Electromechanical Actuators. *Journal of Non-Crystalline Solids* **2016,** *453*, 8-15.

27. Puértolas, J. A.; García-García, J. F.; Pascual, F. J.; González-Domínguez, J. M.; Martínez, M. T.; Ansón-Casaos, A. Dielectric Behavior and Electrical Conductivity of Pvdf Filled with Functionalized Single-Walled Carbon Nanotubes. *Composites Science and Technology* **2017,** *152*, 263-274.

28. Chernousova, S.; Epple, M. Silver as Antibacterial Agent: Ion, Nanoparticle, and Metal. *Angewandte Chemie - International Edition* **2013,** *52*, 1636-1653.

29. Wang, H.; Fu, Q.; Luo, J.; Zhao, D.; Luo, L.; Li, W. Three-Phase Fe3o4/Mwnt/Pvdf Nanocomposites with High Dielectric Constant for Embedded Capacitor. *Applied Physics Letters* **2017,** *110*, 242902.

30. Yadav, D. K.; Yadav, A.; Meena, K.; Devat, K.; Mishra, J. K.; Sahu, R.; Jain, S. K.; Dixit, A.; Srivastava, N.; Patodia, T.; Jakhar, N.; Tripathi, B. Study of Cnt Intercalated Bi2o3/Pvdf Composite for Super Capacitors Applications. *Macromolecular Symposia* **2021,** *399*, 2100022.

31. Mooti, A.; Costa, C. M.; Maceiras, A.; Pereira, N.; Tubio, C. R.; Vilas, J. L.; Besbes-Hentati, S.; Lanceros-Mendez, S. Magnetic and High-Dielectric-Constant Nanoparticle Polymer Tri-Composites for Sensor Applications. *Journal of Materials Science* **2020,** *55*, 16234-16246.

32. Martins, P. M.; Gomez, V.; Lopes, A. C.; Tavares, C. J.; Botelho, G.; Irusta, S.; Lanceros-Mendez, S. Improving Photocatalytic Performance and Recyclability by Development of Er-Doped and Er/Pr-Codoped Tio2/Poly(Vinylidene Difluoride)–Trifluoroethylene Composite Membranes. *The Journal of Physical Chemistry C* **2014,** *118*, 27944-27953.

33. Martins, P.; Kappert, S.; Nga Le, H.; Sebastian, V.; Kühn, K.; Alves, M.; Pereira, L.; Cuniberti, G.; Melle-Franco, M.; Lanceros-Méndez, S. Enhanced Photocatalytic Activity of Au/Tio2 Nanoparticles against Ciprofloxacin. *Catalysts* **2020,** *10*, 234.

34. Alsheheri, S. Z. Nanocomposites Containing Titanium Dioxide for Environmental Remediation. *Designed Monomers and Polymers* **2021,** *24*, 22-45.

35. Martins, P. M.; Ribeiro, J. M.; Teixeira, S.; Petrovykh, D. Y.; Cuniberti, G.; Pereira, L.; Lanceros-Méndez, S. Photocatalytic Microporous Membrane against the Increasing Problem of Water Emerging Pollutants. *Materials* **2019,** *12*, 1649.

36. Jothi Prakash, C. G.; Prasanth, R. 7 - Tio2-Based Devices for Energy-Related Applications. In *Titanium Dioxide (Tio_2) and Its Applications*, Parrino, F.; Palmisano, L., Eds. Elsevier: **2021**, pp 241-265.

37. Serra, J. P.; Fidalgo-Marijuan, A.; Martins, P. M.; Queirós, J. M.; Gonçalves, R.; Gutiérrez-Pardo, A.; Aguesse, F.; Costa, C. M.; Lanceros-Mendez, S. Porous Composite Bifunctional Membranes for Lithium-Ion Battery Separator and Photocatalytic Degradation Applications: Toward Multifunctionality for Circular Economy. *Advanced Energy and Sustainability Research* **2021,** *2*, 2100046.

38. Swathy, J. R.; Udhaya Sankar, M.; Chaudhary, A.; Aigal, S.; Anshup; Pradeep, T. Antimicrobial Silver: An Unprecedented Anion Effect. *Scientific Reports 2014 4:1* **2014,** *4*, 1-5.

39. Salazar, H.; Martins, P. M.; Santos, B.; Fernandes, M. M.; Reizabal, A.; Sebastián, V.; Botelho, G.; Tavares, C. J.; Vilas-Vilela, J. L.; Lanceros-Mendez, S. Photocatalytic and Antimicrobial Multifunctional Nanocomposite Membranes for Emerging Pollutants Water Treatment Applications. *Chemosphere* **2020,** *250*, 126299.

40. Vertuccio, L.; Spinelli, G.; Lamberti, P.; Tucci, V.; Zarrelli, M.; Russo, S.; Iannuzzo, G.; Guadagno, L. Self-Sensing Nanocomposites in Automotive/Aeronautic Field. *Materials Today: Proceedings* **2021,** *34*, 125-127.

41. Lizundia, E.; Maceiras, A.; Vilas, J. L.; Martins, P.; Lanceros-Mendez, S. Magnetic Cellulose Nanocrystal Nanocomposites for the Development of Green Functional Materials. *Carbohydrate polymers* **2017,** *175*, 425-432.

42. Pereira, N.; Gonçalves, S.; Barbosa, J. C.; Gonçalves, R.; Tubio, C. R.; Vilas-Vilela, J. L.; Costa, C. M.; Lanceros-Mendez, S. High Dielectric Constant Poly(Vinylidene Fluoride-Trifluoroethylene-Chlorofluoroethylene) for Capacitive Pressure and Bending Sensors. *Polymer* **2021,** *214*, 123349.

43. Wu, Y.; Hsu, S. L.; Honeker, C.; Bravet, D. J.; Williams, D. S. The Role of Surface Charge of Nucleation Agents on the Crystallization Behavior of Poly(Vinylidene Fluoride). *The Journal of Physical Chemistry B* **2012,** *116*, 7379-7388.

44. Yuan, Q.; Zhang, Y.; Chen, Y.; Wang, R.; Du, C.; Yasun, E.; Tan, W. Using Silver Nanowire Antennas to Enhance the Conversion Efficiency of Photoresponsive DNA Nanomotors. *Proceedings of the National Academy of Sciences* **2011,** *108*, 9331-9336.

45. Martins, P.; Lopes, A. C.; Lanceros-Mendez, S. Electroactive Phases of Poly(Vinylidene Fluoride): Determination, Processing and Applications. *Progress in Polymer Science* **2014,** *39*, 683-706.

46. An, N.; Liu, H.; Ding, Y.; Zhang, M.; Tang, Y. Preparation and Electroactive Properties of a Pvdf/Nano-Tio2 Composite Film. *Applied Surface Science* **2011,** *257*, 3831-3835.

47. Cheon, S.; Kang, H.; Kim, H.; Son, Y.; Lee, J. Y.; Shin, H.-J.; Kim, S.-W.; Cho, J. H. High-Performance Triboelectric Nanogenerators Based on Electrospun Polyvinylidene Fluoride–Silver Nanowire Composite Nanofibers. *Advanced Functional Materials* **2018,** *28*, 1703778.

48. Fernandes, L. C.; Correia, D. M.; Pereira, N.; Tubio, C. R.; Lanceros-Méndez, S. Highly Sensitive Humidity Sensor Based on Ionic Liquid–Polymer Composites. *ACS Applied Polymer Materials* **2019,** *1*, 2723-2730.

49. Li, W.; Li, H.; Zhang, Y.-M. Preparation and Investigation of Pvdf/Pmma/Tio2 Composite Film. *Journal of Materials Science* **2009,** *44*, 2977-2984.

50. Lee, J. G.; Kim, S. H.; Kang, H. C.; Park, S. H. Effect of Tio2 on Pvdf/Pmma Composite Films Prepared by Thermal Casting. *Macromolecular Research* **2013,** *21*, 349-355.

51. Wang, Y.-J.; Kim, D. Crystallinity, Morphology, Mechanical Properties and Conductivity Study of in Situ Formed Pvdf/Liclo4/Tio2 Nanocomposite Polymer Electrolytes. *Electrochimica Acta* **2007,** *52*, 3181-3189.

52. Li, Z.; Zhang, L.; Qi, R.; Xie, F.; Qi, S. Improvement of the Thermal Transport Performance of a Poly(Vinylidene Fluoride) Composite Film Including Silver Nanowire. *Journal of Applied Polymer Science* **2016,** *133*, 43554.

53. Costa, C. M.; Sencadas, V.; Pelicano, I.; Martins, F.; Rocha, J. G.; Lanceros-Mendez, S. Microscopic Origin of the High-Strain Mechanical Response of Poled and Non-Poled Poly(Vinylidene Fluoride) in the B-Phase. *Journal of Non-Crystalline Solids* **2008,** *354*, 3871-3876.

54. Menard, K. P. *Dynamic Mechanical Analysis: A Practical Introduction*. CRC Press: **1999**.

55. Lizundia; E; Fortunati; E; Dominici; F; Vilas; J, L.; Le´on; L, M.; Armentano; I; Torre; L; and, K.; J Plla-Grafted Cellulose Nanocrystals: Role of the Cnc Content and Grafting on the Pla Bionanocomposite Film Properties. *Carbohydrate polymers* **2016**, *142*, 105-113.

56. Raquez, J. M.; Habibi, Y.; Murariu, M.; Dubois, P. Polylactide (Pla)-Based Nanocomposites. *Progress in Polymer Science* **2013,** *38*, 1504-1542.

57. Lizundia, E.; Maceiras, A.; Vilas, J. L.; Martins, P.; Lanceros-Mendez, S. Magnetic Cellulose Nanocrystal Nanocomposites for the Development of Green Functional Materials. *Carbohydrate Polymers* **2017,** *175*, 425-432.

58. Roy, S.; Thakur, P.; Hoque, N. A.; Bagchi, B.; Sepay, N.; Khatun, F.; Kool, A.; Das, S. Electroactive and High Dielectric Folic Acid/Pvdf Composite Film Rooted Simplistic Organic Photovoltaic Self-Charging Energy Storage Cell with Superior Energy Density and Storage Capability. *ACS Applied Materials & Interfaces* **2017,** *9*, 24198-24209.

59. B S, M. S.; Hiremath, S.; Kulkarni, S. M. Influence of Conductive and Dielectric Fillers on the Relaxation of Solid Silicone Rubber Composites. *Materials Research Express* **2019,** *6*, 125308.

60. Arisawa, H.; Yano, O.; Wada, Y. Dielectric Loss of Poly(Vinylidene Fluoride) at Low Temperatures and Effect of Poling on the Low Temperature Loss. *Ferroelectrics* **1981,** *32*, 39-41.

61. Dyre, J. C. The Random Free-Energy Barrier Model for Ac Conduction in Disordered Solids. *Journal of Applied Physics* **1988,** *64*, 2456-2468.

62. Jonscher, A. K. The 'Universal' Dielectric Response. *Nature* **1977,** *267*, 673-679.

63. Fujishima, A.; Zhang, X.; Tryk, D. A. Tio2 Photocatalysis and Related Surface Phenomena. *Surface Science Reports* **2008,** *63*, 515-582.

64. Zhang, H.; Mane, A. U.; Yang, X.; Xia, Z.; Barry, E. F.; Luo, J.; Wan, Y.; Elam, J. W.; Darling, S. B. Visible-Light-Activated Photocatalytic Films toward Self-Cleaning Membranes. *Advanced Functional Materials* **2020,** *30*, 2002847.

FOR TABLE OF CONTENTS ONLY